Available online at www.sciencedirect.com

Chemical Engineering Research and Design

journal homepage: www.elsevier.com/locate/cherd

# Smart paradigm to predict copper surface area of $Cu/ZnO/Al_2O_3$ catalyst based on synthesis parameters

Soheil Saffary[a], Mansoureh Rafiee[b], Mohammadreza Saeidi Varnoosfaderani[a], M. Erdem Günay[c], Sohrab Zendehboudi[d,*]

[a] School of Metallurgy and Materials Engineering, Iran University of Science & Technology, Narmak, Tehran, 1684613114, Iran

[b] Department of Chemical and Petroleum Engineering, Sharif University of Technology, Azadi Ave, Tehran, 1458889694, Iran

[c] Department of Energy Systems Engineering, Istanbul Bilgi University, 34060 Eyupsultan-Istanbul, Turkey

[d] Faculty of Engineering and Applied Science, Memorial University, St. John's, NL A1B 3X5, Canada

ARTICLE INFO

*Article history:*
Received 3 October 2022
Received in revised form
25 December 2022
Accepted 17 January 2023
Available online 20 January 2023

*Keywords:*
Machine learning
Water-gas shift reaction
Methanol steam reforming
Methanol synthesis
$Cu/ZnO/Al_2O_3$ catalyst

ABSTRACT

$Cu/ZnO/Al_2O_3$ catalyst is used in processes of water-gas shift, methanol steam reforming, and methanol synthesis in the industry. According to various experimental studies, the catalytic activity of this catalyst is directly proportional to its copper surface area (Cu(SA)). In this study, a machine learning approach for predicting Cu(SA) ranges in three classes (low, medium, and high) is introduced based on catalyst preparation factors. Three models of random forest (RF), support vector machine (SVM), and multilayer perceptron artificial neural network (MLP-ANN) classifiers are developed and optimized using grid search 10-fold cross-validation for a 188 sample dataset extracted from 45 experimental studies. It is found that the RF classifier with 90% cross-validation accuracy score and 94.7% test data prediction accuracy score outperforms the other two models. The SHAP (or SHapley Additive exPlanations) analysis is performed to investigate the effects of synthesis factors, such as aging conditions, precipitant type, and pH on Cu(SA). It is concluded that Cu/Zn ratio has the greatest influence on Cu(SA). The optimum synthesis conditions yielding high Cu(SA) are also discovered, which is of great importance for synthesis of $Cu/ZnO/Al_2O_3$ catalysts with high catalytic activity.



## 1. Introduction

$Cu/ZnO/Al_2O_3$ is an industrial catalyst for processes such as CO conversion or hydrogen purification through water-gas shift (WGS) reaction ($CO+H_2O \rightarrow H_2 + CO_2$) (Andache et al., 2019; Guo et al., 2009; Sagata et al., 2013), hydrogen production through methanol steam reforming reaction ($CH_3OH+H_2O \rightarrow 3\,H_2 + CO_2$) for fuel cell applications (Khzouz et al., 2013; Lindstrom and Pettersson, 2001; Shokrani et al., 2014; Zhu et al., 2022), WGS reaction in ammonia plants (Schumann, 2015; Studt et al., 2014), and methanol synthesis ($CO+2\,H_2 \rightarrow CH_3OH$) (Behrens et al., 2013b; Saito et al., 1996; Shim et al., 2019).

In general, $Cu/ZnO/Al_2O_3$, also called CZA in this work, is prepared from a mixed oxide powder that includes CuO, ZnO, and $Al_2O_3$. Since the production methods of this powder in the industry are based on precipitation from aqueous solutions of metal salts, the resulted CuO, ZnO, and $Al_2O_3$ particles are nano-sized. Furthermore, precipitation-based

* Corresponding author.
E-mail address: szendehboudi@mun.ca (S. Zendehboudi).

https://doi.org/10.1016/j.cherd.2023.01.031

synthesis pathway provides an ideal mixing homogeneity for these phases. This characteristic causes CuO, ZnO, and $Al_2O_3$ regions to form large common borders with each other (Behrens et al., 2013a). Each of the three phases of CuO, ZnO, and $Al_2O_3$ plays an important role in the catalyst body. In summary, metallic copper is the active site; zinc oxide plays the role of copper dispersant as well as the synergic agent for the catalytic activity (Kim et al., 2020, 2011; Kurr et al., 2008; Pan et al., 1988; Reubroycharoen et al., 2004; Stone and Waller, 2003a,b; Zander et al., 2013); and aluminum oxide carries structural and electronic effects that improve catalyst stability, copper dispersion, and catalytic activity (Guil-López et al., 2020; Kurtz et al., 2003; Mota et al., 2018; Schumann, 2015; Wilmer et al., 2003).

In addition to improvement of the catalyst stability and inherent activity, producers of CZA catalyst make efforts to increase the Cu(SA) value because it has a direct relationship with the catalyst activity. Various research studies have shown that different synthesis factors (e.g., pH and temperature) in the catalyst preparation procedure affect the Cu (SA) value (Behrens et al., 2012; Budiman et al., 2013).

Three synthesis routes are reported for CZA catalysts: co-precipitation (Álvarez Galván et al., 2016; Behrens, 2009; Behrens et al., 2013b; Günter et al., 2001; Sagata et al., 2013; Saito et al., 1996; Stone and Waller, 2003a, 2003b; Schumann et al., 2014; Figueiredo et al., 2011; Meshkini et al., 2010; Samei et al., 2012), deposition-precipitation (Cai et al., 2004; Madon and Nagel, 2009; Zhang et al., 2017), and incipient wetness impregnation (Jeong et al., 2014), among which the co-precipitation is the most frequently reported method. In the co-precipitation synthesis method, an aqueous mixed salt solution of Cu, Zn, and Al is precipitated by an aqueous alkaline solution such as sodium carbonate solution (Kim et al., 2020, 2011; Kurr et al., 2008; Reubroycharoen et al., 2004; Stone and Waller, 2003a,b; Zander et al., 2013), sodium bicarbonate solution (Angelo et al., 2015; Budiman et al., 2013; Kim et al., 2011; Kurtz et al., 2003), ammonium carbonate solution (Smith et al., 2017), or a mixed solution of sodium hydroxide and sodium carbonate (Behrens et al., 2010; Zhang et al., 2010). The precipitation occurs under vigorous stirring, controlled temperature, ambient pressure, and constant or variable pH. The resultant precipitate is usually aged in the mother liquid under stirring. The next step is filtration and washing the resulting cake with deionized water until the impurities, mainly sodium, are eliminated. The produced cake is the catalyst precursor, which should be dried and calcined (usually in an air atmosphere condition) in the next step to obtain the catalyst powder. The resulting catalyst powder is a mixed metal oxide of CuO, ZnO, and $Al_2O_3$ phases plus some carbonate phases remaining from the process. In the industry, the catalyst powder is shaped into tablet, and the reduction step (activation) of CuO to metallic Cu is carried out before the process starts, in the reactor where the catalyst is going to be used (Álvarez Galván et al., 2016; Behrens, 2009; Günter et al., 2001).

CZA catalyst is the most common type of the catalysts used for WGS (CO conversion), methanol synthesis, and methanol steam reforming reactions. This catalyst is employed in the corresponding industry with different ratios of three oxides CuO, ZnO, and Al2O3.

Artificial intelligence / machine learning (AI/ML) techniques have been widely used from the last decade to extract information from huge amount of data available in various fields including chemistry, materials science and engineering, and chemical and petroleum engineering for prediction, classification, and optimization purposes, while it is very costly, time-consuming, or even impossible to obtain such behaviors/information with experimental or mathematical modeling/simulation methods (Chamkalani et al., 2013; Dashti et al., 2019; Ghiasi and Zendehboudi, 2021; Kamari et al., 2014; Miah et al., 2020). For instance, different ML tools have been employed for discovering new information about catalyst design, in terms of chemical composition and synthesis processes (Cavalcanti et al., 2019; Günay et al., 2012; Gunay and Yildirim, 2011; Günay and Yildirim, 2013; Odabaşi et al., 2014; Omata et al., 2001; Umegaki et al., 2008).

Extensive experimental studies have been conducted on synthesis parameters of CZA catalyst to obtain maximum performance, selectivity, and stability (Eduardo et al., 2022; Gherardi et al., 1983; Guil-López et al., 2020; Kim et al., 2020, 2011; Kurr et al., 2008; Kurtz et al., 2003; Mota et al., 2018; Pan et al., 1988; Porta et al., 1988; Reubroycharoen et al., 2004; Schumann, 2015; Smith et al., 2020; Stone and Waller, 2003a, 2003b; Zander et al., 2013). In this research, the ML approaches are used to study the common and industrial preparation method of this catalyst (co-precipitation) so that influences of the synthesis factors on the catalyst Cu(SA) are investigated. Although, there are some ML studies in the literature with focus on prediction of the characteristics of the catalysts used for reactions of WGS, methanol synthesis, and methanol steam reforming, the present study differs from previous studies in terms of the model output (Cu(SA)), the synthesis method, and chemical composition of the catalyst.

Gunay and Yildirim (2011) used an artificial neural network (ANN) to predict CO conversion of Cu-based catalysts based on the catalyst preparation factors (including synthesis route, support type, and calcination condition) and operating parameters (e.g., reaction temperature, feed composition, and feed flowrate/catalyst weight ratio). Günay et al. (2012) also investigated the activity of promoted Pt-$CeO_2/Al_2O_3$ catalysts in WGS reaction through experimental and ANN studies. Their results showed that K promotes the activity, while Co and Ni lower the catalyst performance. In another work, Günay and Yildirim (2013) considered the CO conversion reaction rate on Au-based catalysts as a function of catalyst preparation parameters and operational conditions using an ANN approach. Omata et al. (2001) optimized the catalytic activity of Cu-Zn-Al-Sc catalysts in methanol synthesis reaction through genetic algorithm (GA) combined with ANN. Cavalcanti et al. (2019) optimized the catalytic activity of various types of catalysts for WGS reaction through an ANN strategy based on the synthesis parameters (e.g., active phase and support type) and operation conditions. They concluded that a better catalytic performance is obtained for WGS reaction by using ceria-supported catalysts with active phases of Ru, Ni, or Cu. Umegaki et al. (2008) investigated the activity of Cu-based mixed oxide catalysts for methanol steam reforming reaction using the ANN technique, where the physicochemical properties of the ingredients were the input parameters. They suggested the Cu–Ca binary system, and Cu–Ce–Mn and Cu–Pr–Ti ternary systems as the best candidates. In addition, they optimized the elements' proportions and preparation factors. Odabaşi et al. (2014) investigated the WGS reaction over noble metal catalysts using decision tree (DT), ANN, and support vector machine (SVM) tools while considering wide ranges of input parameters such as types of base metal, support, and promoters. Eduardo et al. (2022) studied the effect of the synthesis factors as well as catalyst cost on the CO

conversion of WGS catalysts through using ANN and random forest (RF) models.

This study evaluates the effect of synthesis factors on Cu (SA) of CZA catalysts. It should be noted that in previous ML-based studies on synthesis factors of Cu-based catalysts, the activity level of the catalysts in various reactions (e.g., WGS, methanol steam reforming, and methanol synthesis) has been taken as the target variable (Cavalcanti et al., 2019; Günay et al., 2012; Gunay and Yildirim, 2011; Günay and Yildirim, 2013; Odabaşi et al., 2014; Omata et al., 2001; Umegaki et al., 2008), while in the present work, Cu(SA) of the catalyst is considered as the objective function. The reason for this choice is twofold: firstly, it is experimentally proven that the Cu(SA) of CZA catalyst samples with the same preparation method is nearly linearly correlated with their catalytic activity (Behrens et al., 2012; Budiman et al., 2013; Dasireddy and Likozar, 2019; Fujita et al., 2001; Fujitani and Nakamura, 1998; Jeong et al., 2017; Kniep et al., 2005; Kurtz et al., 2004; Reubroycharoen et al., 2004; Sagata et al., 2013; Saito et al., 1996; Shishido et al., 2006); Secondly, there is an advantage in choosing Cu(SA) over catalytic activity as the target variable, which stems from the fact that Cu(SA) is an intrinsic characteristic of the catalyst; however, level of catalyst activity depends on the measurement conditions such as gas velocity, temperature, pressure, inlet gas composition and flow rate, sample shape (powder or tablet), mesh size, and sample bed size, some of which have not been even reported for some applications in the literature. In addition, among the 8 synthesis factors that are considered in this study as the features, four factors including, pH mode (which specifies the mixing order of solutions in the co-precipitation process), precipitant, aging time, and temperature have not been investigated in the previous modeling works so far.

Previous studies have investigated various catalyst candidates for the WGS, methanol synthesis, and methanol steam reforming reaction with different support types, promoters, and synthesis methods, while this study sheds light on the preparation of catalysts with $Cu/ZnO/Al_2O_3$ composition which are the main industrial catalysts for the mentioned reactions in petrochemical and refinery plants (Behrens et al., 2013a; Cai et al., 2004; Madon and Nagel, 2009). In this research, the catalyst composition is limited to $Cu/ZnO/Al_2O_3$ mixed oxide (without any promoter), the synthesis method is limited to co-precipitation, which is the most common industrial method for producing this catalyst, the source metals forming the catalyst are limited to nitrate salts, which are the conventional metal source for preparing this catalyst in the industry, and the precipitant is either sodium carbonate ($Na_2CO_3$) or sodium bicarbonate ($NaHCO_3$) solution.

In this research, the target value of Cu(SA) is classified into three classes (low, medium, and high) and the problem is solved in the classification mode. Three models of SVM, MLP-ANN, and RF classifiers are employed for predicting the Cu(SA) class. The best model that has the highest cross-validation accuracy score and test data prediction accuracy score, is used for analyzing the effect of features in the SHAP (SHapley Additive exPlanations) analysis.

## 2. Literature summary

Eight synthesis factors used in this study as the input features are described below in terms of their effect on Cu(SA). This section includes all the experimental studies on these factors and their effects on Cu(SA) and catalyst activity.

### 2.1. *Cu/Zn*

In the synthesis of CZA catalyst, the Cu/Zn ratio plays a critical role in the type of precipitate phases forming in the catalyst precursor. The possible phases in the precipitate include malachite ($Cu_2(OH)_2CO_3$), zinc malachite ($(Cu,Zn)_2(OH)_2CO_3$), aurichalcite ($(Cu,Zn)_5(OH)_6(CO_3)_2$), hydrozincite ($Zn(OH)_6(CO_3)_2$), and hydrotalcite ($(Cu,Zn)_6Al_2(OH)_{16}CO_3{\cdot}4\,H_2O$) (Bems et al., 2003; Fujitani and Nakamura, 1998; Guil-López et al., 2020; Pospelova et al., 2019; Stone and Waller, 2003a,b; Waller et al., 1989). Various studies have shown that the formation of each of the precipitate phases (pure or mixture) leads to a specific range of Cu(SA) for the final catalyst (Álvarez Galván et al., 2016; Behrens, 2009; Fujitani and Nakamura, 1998; Günter et al., 2001; Mota et al., 2018; Pospelova et al., 2020; Stone and Waller, 2003a,b). Various values for the Cu/Zn ratio to attain the maximum Cu(SA) have been reported. For catalysts in the CZ system or CuO/ZnO (without aluminum), the reported optimal Cu/Zn ratios are: 2/1 (Stone and Waller, 2003a,b), 2.6 (Behrens, 2009), 2.3 (Günter et al., 2001), 1 (Álvarez Galván et al., 2016; Reubroycharoen et al., 2004), 1.28 (Fujitani and Nakamura, 1998), and the optimal ratios for the CZA system are 4.3 for 20% Al (Stone and Waller, 2003a, 2003b), 1 for 14.3% Al (Budiman et al., 2013), and 2 for both 25% and 66.7% Al (Kim et al., 2011).

### 2.2. *Al%*

Various experimental studies have shown that adding Al to CZ system promotes copper dispersion and increases Cu(SA), although its excessive content/concentration can cause a drop in Cu(SA), which is due to the formation of hydrotalcite-like phase (Cai et al., 2003; Gusi et al., 1985; Park et al., 2018; Saito et al., 1996; Xu et al., 2018). It was found that the optimal value of Al is not independent of Cu/Zn ratio and alters with this ratio. The reported optimum values for Al content are 3% for Cu/Zn= 2.3 (Guil-López et al., 2020), 3.3% for Cu/Zn= 2.7 (Kim et al., 2020), 2.4% for Cu/Zn= 0.95 (Xu et al., 2018), and 4% for Cu/Zn= 2.3 (Behrens et al., 2013b). Also, Schumann (2015) showed that 2% Al addition to a CZ catalyst with Cu/Zn= 0.67 increases the Cu(SA) from 21 to 27 $m^2$/g.cat. Jeong et al. (2017) reported that 14% Al addition to a CZ catalyst with Cu/Zn= 2.4 increases the Cu(SA) from 16 to 25 $m^2$/g.cat. Park et al. (2018) concluded that 3% Al addition to a CZ catalyst with Cu/Zn= 2.3 increases the Cu(SA) from 10 to 20 $m^2$/g.cat. Wang et al. (2010) found that 10% Al addition to a CZ catalyst with Cu/Zn= 2 increases the Cu(SA) from 19 to 54 $m^2$/g.cat. Stone and Waller (2003a, 2003b) showed that Cu(SA), which is very low for CZ catalysts with high Cu/Zn, significantly increases upon the addition of Al.

### 2.3. *Aging time*

Experimental investigations have proven that a minimum aging period is required for some favorable phase transformations which result in a homogeneous microstructure and high Cu(SA) for the final catalyst. There is no report or technical document in the literature, claiming that a very long aging time has a negative effect on catalyst activity. Indeed, the literature reveals that incomplete aging and phase transformation lead to low Cu(SA) as well as low catalytic activity for the final catalyst (Farahani et al., 2014; Kniep et al., 2005; Mota et al., 2018; Spencer, 2000; Waller et al., 1989). Various research studies have shown that at an aging temperature of about 60 °C (the most frequently

reported aging temperature), an aging time of 2.5 hr is long enough to complete the favorable phase transformations and reach the highest Cu(SA); however, longer aging times are needed for significantly lower aging temperatures to complete the phase transformations (Farahani et al., 2014; Kniep et al., 2005; Mota et al., 2018; Waller et al., 1989). Farahani et al. (2014) found that the 24 hr is an adequate aging time when the aging temperature is as low as 40 °C.

### 2.4. *Aging temperature*

Various aging temperatures for the synthesis of CZA catalyst have been reported in open sources, ranging from 60 °C to 70 °C. There are a few studies that have focused on the effect of aging temperature on Cu(SA). Farahani et al. (2014) selected 40 °C, 60 °C, and 80 °C as the aging temperature for a CZ precursor with Cu/Zn= 2. They concluded that 60 °C is the optimum aging temperature to obtain the maximum Cu(SA) for the final catalyst. Spencer (2000) and Farahani et al. (2014) found that low aging temperatures significantly lower the rate of the favorable phase transformations in the precipitate.

### 2.5. *pH mode*

Typically, an alkaline precipitant solution is mixed with an acidic mixed metal salt solution in a co-precipitation synthesis process (Álvarez Galván et al., 2016; Behrens, 2009; Günter et al., 2001). A more detailed description of the co-precipitation process is given in the introduction section. There are three common addition modes for mixing the acidic and basic solutions, including: a) decreasing pH mode so that acidic mixed metal solution is added to the alkaline precipitant solution. This addition mode is labeled 'decreasing' pH mode, which indicates the state of pH changes in the synthesis vessel during the addition; b) constant pH mode, which means simultaneous addition at a rate that keeps the pH value constant inside the vessel during addition; and c) increasing pH mode so that alkaline precipitant solution is added to the acidic mixed metal solution (Álvarez Galván et al., 2016; Behrens, 2009; Budiman et al., 2013; Günter et al., 2001; Pan et al., 1988). Among these pH modes, the ‘constant’ mode (Andache et al., 2019; Behrens, 2009; Behrens et al., 2013a; Breen and Ross, 1999; Dasireddy and Likozar, 2019; Farahani et al., 2014; Fierro et al., 2002a, 2002b) and ‘decreasing’ mode (Budiman et al., 2013; Gusi et al., 1985; Jeong et al., 2017; Kim et al., 2020; Pan et al., 1988; Park et al., 2018; Sagata et al., 2013; Shen et al., 1997; Wang et al., 2010; Xu et al., 2018) are the most frequently reported ones. Pan et al. (1988) and Irandoukht et al. (2000) investigated the influence of pH modes on the catalyst activity and Cu(SA). Pan et al. (1988) showed that the Cu(SA) of CZ catalysts decreases in the following order with respect to the pH mode: 'constant'; Cu(SA) = 60 $m^2$/g.cat > 'decreasing'; Cu(SA)= 33 $m^2$/g.cat > > 'increasing'; Cu(SA)=1.1 $m^2$/g.cat. Irandoukht et al. (2000) concluded that 'decreasing' pH mode leads to higher activity for the CZA catalyst than 'constant' pH mode. Pan et al. (1988) and Stone and Waller (2003a, 2003b) found that pH mode strongly affects the relative precipitation rate of Cu and Zn and consequently the precipitate type and Cu(SA).

### 2.6. *Precipitant*

Based on the literature (Álvarez Galván et al., 2016; Behrens, 2009; Behrens et al., 2013b; Günter et al., 2001; Sagata et al., 2013; Saito et al., 1996; Stone and Waller, 2003a,b) and registered patents by the largest producers of this catalyst such as Sud-Chemi (Behrens et al., 2013a; Cai et al., 2004) and BASF (Madon and Nagel, 2009), it can be concluded that the most frequently reported precipitant for the co-precipitation-based synthesis of CZA catalysts is sodium carbonate ($Na_2CO_3$). The second most frequently used precipitant is sodium bicarbonate ($NaHCO_3$) (Angelo et al., 2015; Budiman et al., 2013; Kim et al., 2011; Kurtz et al., 2003). To the best of our knowledge, only one report has compared the effects of these two precipitants on the final catalyst properties (Chinchen et al., 1987). Based on this study, sodium carbonate results in more activity for the CZA catalyst than sodium bicarbonate.

### 2.7. *Calcination time*

In the catalyst production process, the precipitate obtained from the co-precipitation stage (precursor) is calcined after drying to convert the hydroxycarbonate phases into metal oxides and obtain the catalyst powder (Behrens, 2009; Budiman et al., 2013; Mota et al., 2018; Stone and Waller, 2003a,b). Various calcination times have been reported from 1 hr to 24 hr for CZA catalysts (Xu et al., 2018; Gusi et al., 1985). Irandoukht et al. (2000) studied the effect of calcination time on catalyst quality; it was concluded that longer calcination times promote catalytic activity.

### 2.8. *Calcination temperature*

The reported calcination temperatures for CZA catalysts are mainly between 300 °C and 350 °C. Based on the literature, increasing the calcination temperature above 400 °C decreases the Cu(SA) value due to copper sintering (Álvarez Galván et al., 2016; Behrens, 2009; Budiman et al., 2013; Günter et al., 2001; Schumann, 2015). Sagata et al. (2013) found that increasing the calcination temperature from 400 °C to 500 °C causes 20% and 50% decrease in Cu(SA) for CA ($CuO/Al_2O_3$) and CZ catalysts, respectively. Schumann (2015) calcined CZA catalyst precursors with different Cu/Zn ratios of 2.5 and 0.67 at three different temperatures of 330 °C, 420 °C, and 520 °C. They observed that the Cu(SA) drops by 10% and 42%, respectively, with increasing the calcination temperature for the catalyst with Cu/Zn= 2.5%, and 4% and 49% for the catalyst with Cu/Zn= 0.6. The research study by Farahani et al. (2014) showed a 42% decrease in Cu(SA) by increasing the calcination temperature from 327 °C to 427 °C for the CZ catalyst. According to Pospelova et al. (2020), Cu(SA) for the CZ catalysts with Cu/Zn ratios of 5.1, 1.57, and 0.8 decreases by 28%, 38%, and 50%, respectively, upon an increase in calcination temperature from 300 °C to 450 °C.

## 3. Input data

The dataset used for this work is gathered from 45 research studies and patents. The data bank contains 188 samples of CZA catalysts synthesized through co-precipitation method. It includes eight features which are the preparation factors and one target which is the Cu(SA) class. Further information related to the features and the target is given in Table 1. The target value of Cu(SA) is classified into three classes as low ($0 \leq$ Cu(SA) $< 15\ m^2.g^{-1}$), medium ($15 \leq$ Cu(SA) $< 40\ m^2.g^{-1}$), and high ($40 \leq$ Cu(SA) $< 90\ m^2.g^{-1}$). It should be noted that all the Cu(SA) values extracted from the published articles have been measured by the common titration method of Reactive Frontal Chromatography (RFC) (Chinchen et al., 1987).

**Table 1 – Features and input ranges.**

| Features | Type | Input ranges | Labels |
|---|---|---|---|
| Cu/Zn | Numerical | 0-20.46 | |
| Al % | Numerical | 0-94.76 atomic % | |
| Precipitant | Categorical | Sodium bicarbonate | 0 |
| | | Sodium carbonate | 1 |
| pH mode | Categorical | Constant | 0 |
| | | Decreasing | 1 |
| | | Increasing | 2 |
| Aging temperature | Numerical | 20-85 °C | |
| Aging time | Numerical | 0-65 hr | |
| Calcination temperature | Numerical | 300-520 °C | |
| Calcination time | Numerical | 1-24 hr | |
| **Target** | | | |
| Copper surface area (Cu(SA)) | Categorical | $0 \leq \ldots < 15$ ($m^2.g^{-1}$) | Low |
| | | $15 \leq \ldots < 40$ ($m^2.g^{-1}$) | Medium |
| | | $40 \leq \ldots < 90$ ($m^2.g^{-1}$) | High |

The heat map correlation of the feature-feature and feature-target is shown in Fig. 1. As can be seen from Fig. 1, the feature-feature correlations vary from 0.01 to −0.7. The large value of −0.7 corresponds to the correlation between features 5 and 6 (aging temperature and aging time), because longer aging times are usually chosen in experimental studies when the aging temperature is relatively low. An important conclusion that can be drawn from the heat map correlation is that non-linear models ought to be chosen for modeling the dataset, since the feature-target correlations are small (mostly close to zero and the largest is 0.23).

## 4. Modeling and methodology

The three models of RF, SVM, and MLP classifiers are used in this research. The theory/specifications of these models are briefly explained in the following subsections. In this work, Python programming language and Scikit-learn, Matplotlib, SHAP, and Seaborn free libraries are used to write the codes and draw the graphs/figures.

### 4.1. *Classification models*

#### 4.1.1. *Random forest (RF) classifier*

RF classifier, as its name implies, contains a set of decision trees and acts as an ensemble. From each of the trees, one class is taken out as the answer, and the class with the most votes is chosen as the final output of the RF classifier (Ghiasi and Zendehboudi, 2021). In general, RF has a better performance than decision trees, which are the bricks that make up RF. In fact, decision trees are prone to problems of instability, high variance (overfitting), and bias, which can be overcome by using the ensemble of RF. The reason that the overfitting problem does not occur in RF is averaging of the results of the decision trees (Ghiasi and Zendehboudi, 2021). In RF, the Bootstrap sampling method is used, in which each tree is fed with a random subset of the dataset, and the final prediction is obtained by averaging the results of all trees (Golbabaei et al., 2022).

#### 4.1.2. *Support vector machine (SVM) classifier*

In general, the SVM algorithm finds a hyperplane in the n-dimensional space (n is the number of features) that classifies the data points space (Arabloo et al., 2015; Kamari et al., 2015). There are different hyperplanes to separate two classes in a data space. The goal of the SVM algorithm is to find the hyperplane with the largest margin. The larger the margin is, the more reliable the prediction by the model will be. Indeed, the hyperplane is a decision boundary for classifying data, depending on which side of this boundary the data falls on. The dimension of the hyperplane depends on the number of features (Safari et al., 2014; Zendehboudi et al., 2018). When the number of features is two, the hyperplane is a line. For three

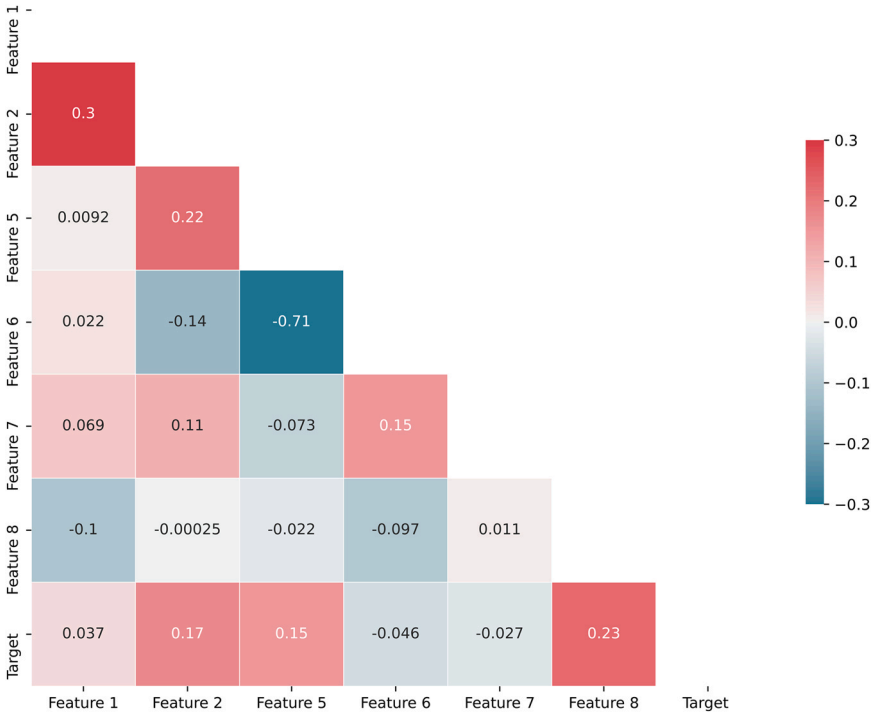


**Fig. 1 – Heat map correlation of features and target.**

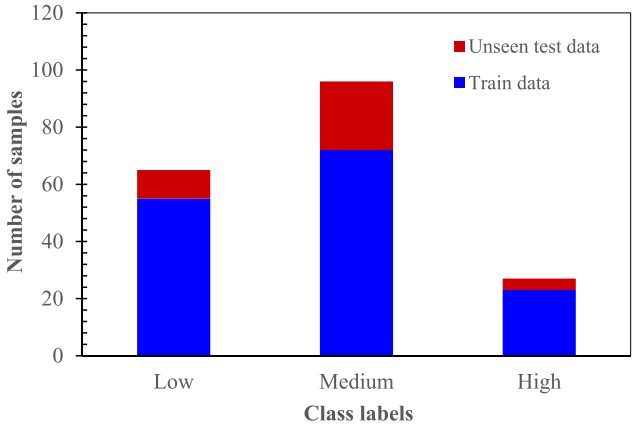


**Fig. 2 – Distribution of sample population in classes.**

features, the hyperplane is a two-dimensional plane. For more features, the dimensions of the hyperplane will increase in the same order. In addition to solving linear problems, SVMs are able to solve non-linear problems using the Kernel trick. Further details about the SVM algorithm can be found in Zendehboudi et al. (2018) and Kamari et al. (2015). One of the important advantages of the SVM approach is its good performance for datasets with high dimensions (large number of features) and small number of samples. However, the main disadvantage of the SVM is its high sensitivity to data preprocessing and tuning of the hyperparameter (Kamari et al., 2015). It is worth mentioning that tree-based models such as RF require minor or no data preprocessing.

#### 4.1.3. *MLP classifier*

Artificial neural network (ANN) is a computing system that is designed based on biological neuron system in the brain. ANN has different types, including convolutional neural network (CNN), recurrent neural network (RNN), and multilayer perceptron (MLP) (Zendehboudi et al., 2018). The last type is used in this study. In the MLP structure, there are one or more hidden layers between the input and output layers. The input layer contains a group of neurons $\{x_i|x_1, x_2, \ldots, x_m\}$, each representing an input feature of the dataset. Each hidden layer receives the information of the previous layer in the form of a weighted linear summation function $w_1x_1+ w_2x_2 +\ldots + w_mx_m$, and it transfers the information to the next layer after applying a non-linear activation function on it. The output layer receives the information from the last hidden layer and expresses it as the output values of the machine (Talebi et al., 2014; Zendehboudi et al., 2018). This algorithm, which is used in the MLP, is a feedforward algorithm where the direction of information flow is from the input layer to the output layer. The most important advantage of ANN is its ability to capture information from large amounts of data and build complex models. The main drawback of an ANANN model is the difficulty of tuning the model parameters (Ghiasi et al., 2015; Golbabaei et al., 2022).

### 4.2. *Data preprocessing*

In this smart modeling study, at first 20% of the total data with 188 samples is set aside as the unseen test data, and the model predictive performance on the unseen test data is determined after training the models based on the remaining 80% of the data points. Before training the models, it should be mentioned that the distribution of samples in the classes is imbalanced (Fig. 2). In order to balance all the classes in the training phase, repeated virtual samples are generated through the sklearn.resample function ("sklearn.utils.resample — scikit-learn 1.1.3 documentation," n.d.). After performing the resampling and increasing the size of classes with smaller populations to the size of the largest class, the total number of samples in the training step is 216 (72 for each class). It should be mentioned that resampling operation is conducted after splitting the main data into training and testing data to prevent data leakage to the testing data.

The last step of data preprocessing is features' standardization. Usually, features have different ranges of variance which can cause errors in the training process of model functions. To solve this problem, the data is generally standardized before being used. In this research, the data is

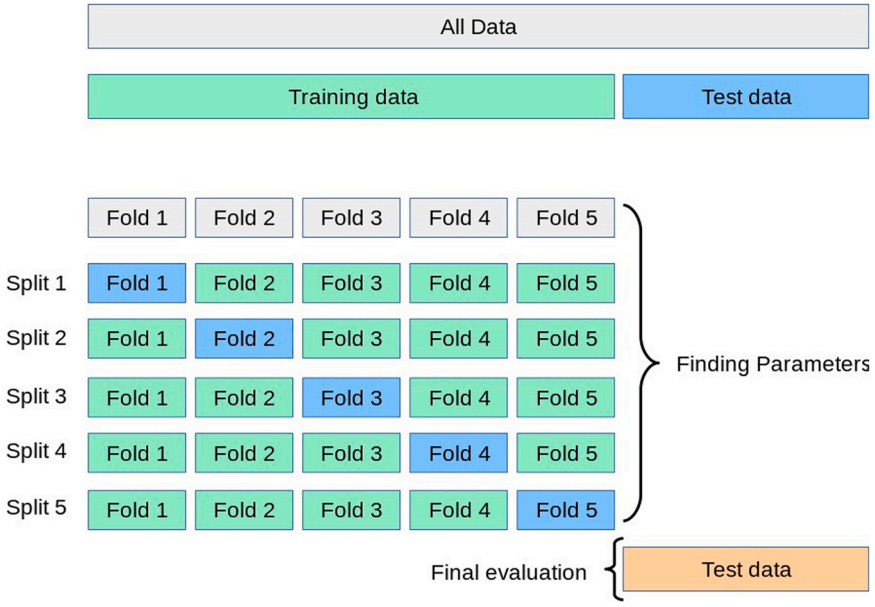


**Fig. 3 – Schematic of cross-validation procedure ("Cross-validation: evaluating estimator performance — scikit-learn," n.d.).**

**Table 2 – Models scores and optimized parameters.**

| Model | Cross-validation accuracy score | Test data accuracy score | Optimized parameters |
|---|---|---|---|
| RF classifier | 90 | 94.7 | Number of estimators= 30 |
| SVM classifier | 87.5 | 65.5 | decision_function_shap= ovr, kernel= rbf, gamma= 50, C= 1 |
| MLP classifier | 80.6 | 82.7 | Activation function= relu, solver= adam |

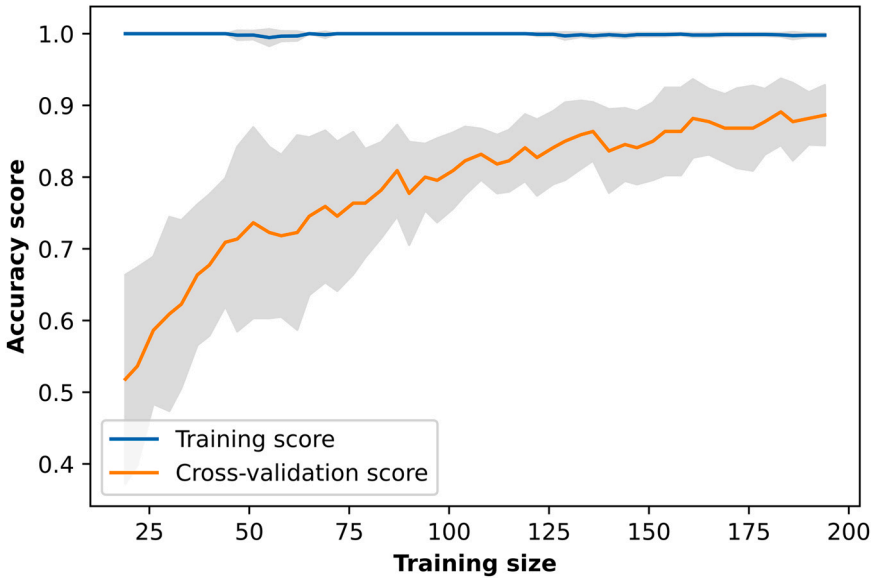


**Fig. 4 – Learning curve of the RF classifier model.**

standardized using the StandardScaler method ("sklearn.preprocessing.StandardScaler — scikit-learn 1.1.3 documentation," n.d.), and all the features' columns of the dataset obtain unit variances and zero mean.

### 4.3. *Modelling procedure*

The training stage is performed by the k-fold cross-validation method with k = 10 and the sampling method of Stratified Shuffle Split. The training data is randomly divided into 10 equal parts. After implementing training on 9 parts of the data, the model is validated using the tenth part, and a validation accuracy score is obtained. After repeating the same procedure for all the 10 folds, 10 validation scores are determined. The average of these scores is the cross-validation accuracy score. The schematic of this procedure is shown in Fig. 3. In addition, each of the models used in this work has specific parameters whose optimal values and types are essential for achieving the maximum accuracy and reliability. Finding these parameters is done through using grid search tuning technique. To do so, different parameters are tested in different ranges so that parameters offering the best cross-validation scores are discovered. After finding the best cross-validation accuracy scores for the models based on their best parameters, the model performance is measured using unseen data points to obtain the prediction accuracy of the testing phase.

In this study, the confusion matrix is used to examine the prediction capability of the model for the unseen data in all classes, as demonstrated in Fig. 3. Finally, SHAP analysis is used to determine the effects of each of the features on the target variable (Cu(SA)).

## 5. Results and discussion

### 5.1. *Comparison of model performances*

The cross-validation accuracy score using the 10-fold cross-validation function and then testing phase prediction accuracy scores are calculated for the RF, SVM, and MLP classifiers. Also, grid search technique is employed to find the optimal parameters and kernels for the models. The results show that the RF classifier outperforms the other two models in both cross-validation accuracy score (90%) and test data prediction accuracy score (94.7%) (Table 2). The grid search

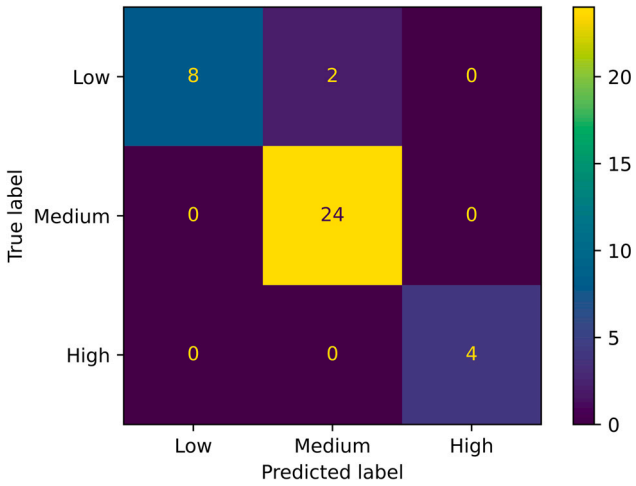


**Fig. 5 – Confusion matrix of the RF classifier model for the testing phase.**

**Table 3 – Confusion matrix metrics of the RF classifier model for the test data.**

| Class label | Precision | Recall | f1-score | Support |
|---|---|---|---|---|
| Low | 1 | 0.8 | 0.89 | 10 |
| Medium | 0.92 | 1 | 0.96 | 24 |
| High | 1 | 1 | 1 | 4 |

results reveal that 30 estimators is the optimal number of estimators for the RF classifier model. The optimal parameters for the SVM model are as follows: decision_function_shap= ovr, kernel= rbf, gamma= 50, and C= 1. Employing the MLP classifier model, two hidden layers with 20 and 10 neurons, 'relu' activation function, and 'adam' solver give the best scores. In the following, the RF classifier which has the best performance is used for further analysis.

Sensitivity analysis is performed to check the sensitivity of the RF classifier model to the synthesis factors (e.g., Cu/Zn, Al%, precipitant, pH mode, aging temperature, aging time, calcination temperature, and calcination time), and the ranking of the parameters/features is as follows [1, 1, 5, 3, 2, 1, 4, 1]. The model shows the least sensitivity to the precipitant and the greatest sensitivity to features of Cu/Zn, Al%, aging time, and calcination time.

### 5.2. *Learning curve*

Learning curve is a criterion for evaluating whether the number of samples is sufficient for training the model or not. To draw this diagram, different subsets of the total data from small to large sizes are separated and used for cross-validation. As expected, the prediction accuracy of the models increases with increasing the training size. When the training size is large enough, the learning curve becomes horizontal, and the cross-validation accuracy does not improve anymore with increasing the training size. If the learning curve is not horizontal yet, it is concluded that more samples are needed in order to reach the maximum accuracy. More information about this diagram in this study is as follows: Subsets of certain sizes are separated randomly from the total train data, which contain 216 members, using the shuffle split method. The size of these subsets is equal to $n \times 216$, where the value of $n$ increases from 0.1 to 1 with an increment of 0.018. After each subset separation, a cross-validation operation with n_splites= 10 is performed to obtain a mean cross-validation score and a training accuracy score using the RF classifier model. Also, a pair of cross-validation and training scores are obtained for all the subsets based on which we can draw the learning curves (Fig. 4). As can be seen, the growth rate of the cross-validation accuracy score decreases upon an increase in the training size and the graph approaches the horizontal state, implying the maximum possible of the accuracy score has been reached for this model and the training size is large enough.

### 5.3. *Confusion matrix*

The confusion matrix in Fig. 5 shows the prediction results of the RF classifier for the testing data of each class. Also, the criteria of precision, recall, and f1-score for each class are given in Table 3. The horizontal axis of the confusion matrix represents the predicted labels of the samples in each class, and the vertical axis represents the true labels of the samples. The numbers in the squares are the number of samples. In the ideal case of 100% accuracy for the model, the non-zero numbers are all in the main diameter of the matrix and other squares are zero. According to Fig. 5, the model mixes up some samples between the classes low and medium, but its prediction performance for the class high is 100%. Table 3 provides further useful information for a better analysis of the model performance.

Suppose a binary model with negative and positive classes, precision shows that from all the classes we have predicted as positive, how many are truly positive (Eq. (1)); and recall shows that how many of all positive classes we have predicted correctly (Eq. (2)) (Chawla et al., 2002; Giussani, 2019). The model is perfect when both of these factors are 1 or 100%. For a better comparison of the model performance in each class, factor f1-score is used, which consists of the harmonic mean of precision and recall (Eq. (3)). Based on Table 3, f1-score for class high is 1, but for two classes of low and medium, it is slightly far from ideal.

$$\text{Precision} = \frac{TP}{TP + FP} \tag{1}$$

$$\text{Recall} = \frac{TP}{TP + FN} \tag{2}$$

$$f1 - \text{score} = 2\frac{\text{Precision} \times \text{Recall}}{\text{Precision} + \text{Recall}} \tag{3}$$

where TP = true-positive, FP = false-positive, and FN = false-negative.

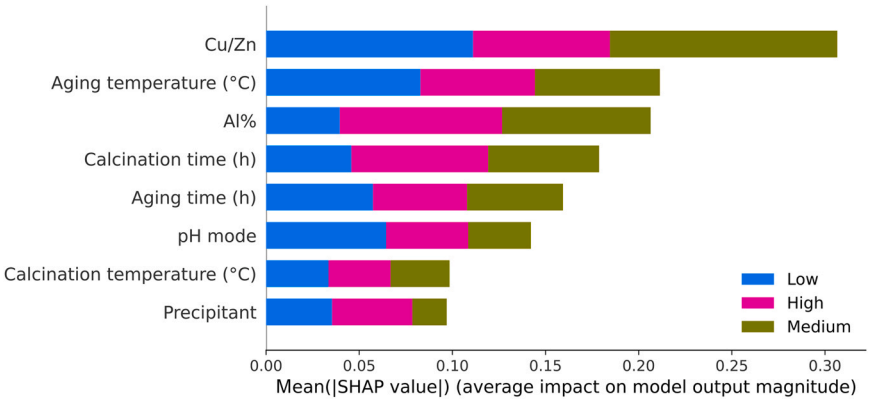


**Fig. 6 – SHAP feature importance plot.**

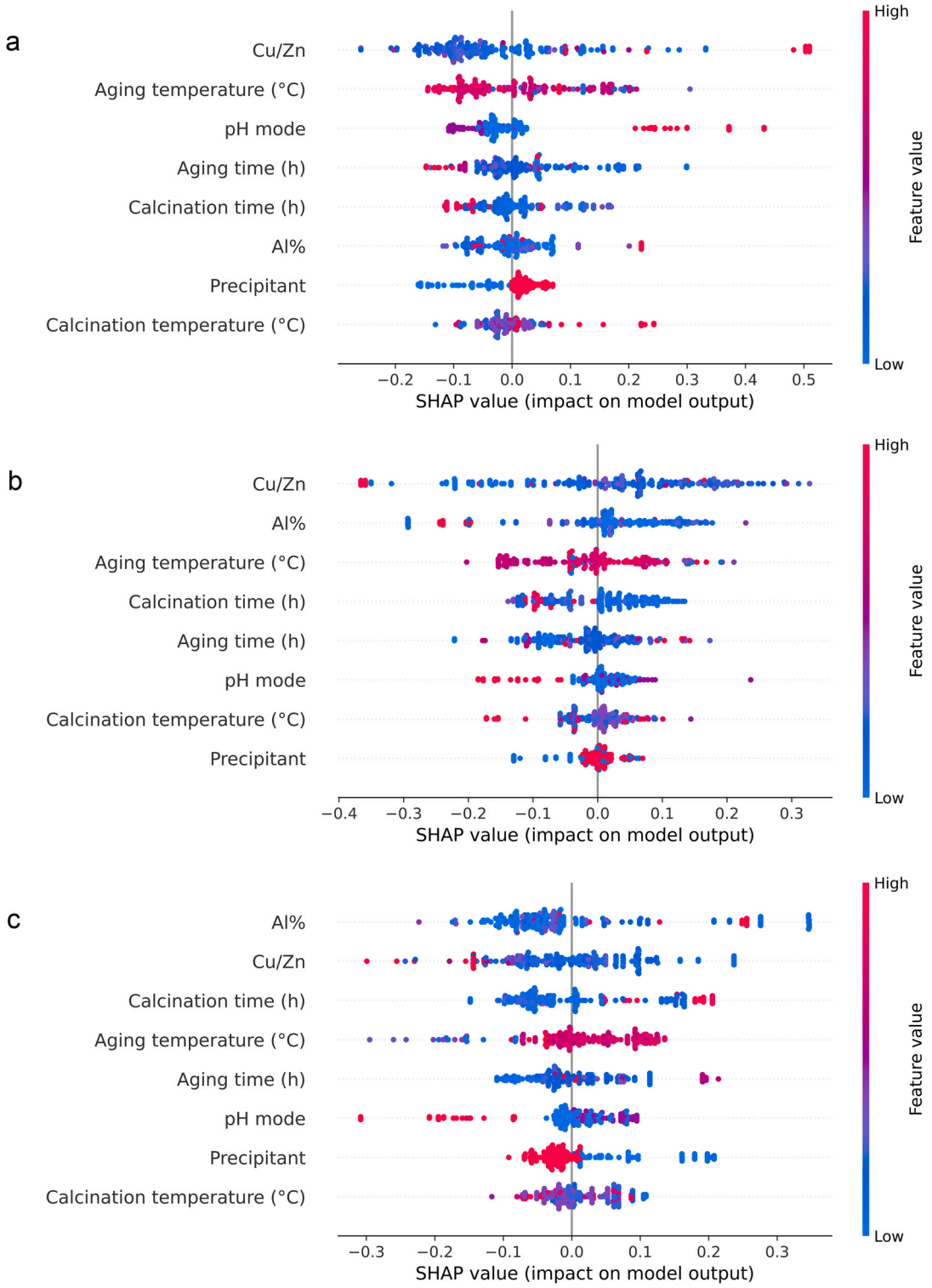


**Fig. 7 – SHAP summary plots (a) class low, (b) class medium, and (c) class high.**

### 5.4. *SHAP analysis*

SHAP (SHapley Additive exPlanations) analysis is one of the recent analytical tools that brings transparency to the models. This analysis, proposed by Lundberg and Lee (2017), explains individual predictions based on Shapley values optimized by game theory (Christoph, 2020; Giussani, 2019; Lundberg et al., 2020; Lundberg and Lee, 2017).

Two types of plots 'SHAP feature importance plot' and 'SHAP summary plot' are used in this study to interpret the model output. SHAP feature importance plot shows the impact of each feature in the model for each class and in total. Feature importance is calculated based on the SHAP values; the greater is the absolute SHAP value for a feature, the greater is its importance. The SHAP feature importance plot in Fig. 6 shows that Cu/Zn is the most effective factor in the model. In other words, Cu/Zn is the most effective synthesis factor for tuning the Cu(SA). Following this factor, the two factors of aging temperature and Al% have the greatest impact on the model response.

The SHAP summary plot shown in Fig. 7 is used to understand the relationship between the features and the target. It should be noted that each of the colored dots indicates the SHAP value of a sample of dataset. For example, if the aging time is too long, we can find out from Fig. 7 what range of Cu(SA) is more likely to be obtained for the final catalyst (high, low, or medium). We can also determine the appropriate range of aging time if a very high Cu(SA) is the goal (see Fig. 7 and Table 1). The changes in the color of the points in these plots represent the feature value so that the blue color corresponds to a low value and the red color shows a high value. For example, in the case of feature 'aging time', the green color indicates short aging times, the red color shows long aging times, and the purple color refers to average aging times. Another important point about these plots is that the more positive the SHAP value is, the higher the probability of happening the class will be. On the contrary, the more negative the SHAP value is, the lower the probability of happening the class will be. In each plot, a vertical middle line passes through the zero point. The points that are on the left side of the vertical line have a negative SHAP value and the points that are on the right side of the vertical line have a positive SHAP value. For example, based on Fig. 7-a, if the goal is not to have the catalyst in the class low, the aging time should be long.

Regarding the two categorical features of precipitant and pH mode (Table 1), the red color corresponds to the larger codes, and the blue color is attributed to the smaller codes. For the case of precipitant, the code '0′, which is related to sodium bicarbonate, has the blue color and the code '1′, which is related to sodium carbonate, has the red color. For the feature of pH mode, code 0, which shows 'constant' pH mode, has the blue color; code 1, which refers to 'decreasing' pH mode, has the violet color; and code 2, which introduces 'increasing' pH mode, has the red color. It should be mentioned that in some classes for the features it is not possible to make a firm judgment about their effect due to mixing of the colors, which originates from the complexity of the system and probably the relatively small size of input data in this research. It is clear when separation of the colors is significant, the factor effect can be assessed well.

It is possible to make a firm judgment about some features' effects based on the plot in Fig. 7-a. To avoid this unfavorable class, which is achieved by standing on the negative side of the SHAP value axis, the type of precipitant should be sodium bicarbonate, the pH mode should be the 'decreasing' mode (violet color), or even 'constant' mode (blue points), and the aging time should be long. Other features such as calcination temperature and time can be judged with some uncertainty. Since most of the red points are on the left side of the vertical line, most likely it will be safe to consider high calcination times to prevent this class to happen. Also, since the red points are relatively far from the vertical line (on the right side), a high calcination temperature helps this class to occur, which is not desirable. It seems that a low aging temperature and a high Cu/Zn ratio should not be chosen for preventing this class to happen. It is not possible to comment on the feature Al% for this class.

According to Fig. 7-b for class medium, it can be concluded that 'increasing' pH mode and high calcination time lower the chance of this class occurrence. It is not possible to comment on other features. For the case of class high in Fig. 7-c, more features can be evaluated with a higher confidence. For instance, if the occurrence of this class or a high Cu(SA) is the target, the precipitant should be sodium bicarbonate instead of sodium carbonate, the pH mode needs to be 'decreasing' and probably 'constant', the aging temperature should not be low, and the calcination time should be long. It can also be claimed that the Cu/Zn ratio should not be very high for this class to occur. It is not possible to make a firm judgment about other features of this class.

Analyzing the overall trends for different features, in most cases they are in agreement with experimental reports and in a few cases in contradiction with experiments. It is revealed that the ratio of Cu/Zn should not be too large to reach medium (0–15 $m^2.g^{-1}$) or high (15–40 $m^2.g^{-1}$) Cu(SA)s for the catalyst. The reduction of Cu(SA) at high values of Cu/Zn ratio is in agreement with the experimental studies (Behrens, 2009; Günter et al., 2001). High or medium aging temperatures (20–85 °C) are suitable for achieving high Cu(SA). This finding is consistent with the experimental results (Farahani et al., 2014; Spencer, 2000). The SHAP feature importance plot in Fig. 6 shows that the effect of calcination time on the model's response (Cu(SA)) is significantly greater than calcination temperature. The same conclusion was drawn in a research investigation (e.g., deep learning) conducted by Eduardo et al. (2022) using a wide range of WGS catalysts where ANN and RF models were implemented. In their research, the catalyst activity is the target parameter, while the target variable is Cu(SA) in the present research. A linear relationship between these two factors has been proven in various experimental works. Thus, it can be concluded that the result obtained in the current study is in agreement with the finding achieved by Eduardo et al. (2022). In other words, the result obtained in this research is in agreement with the finding from the work by Eduardo et al. (2022). The SHAP analysis reveals that long calcination times should be chosen to achieve a high Cu(SA) for the catalyst. The positive effect of long calcination time on the catalyst activity was reported in an experimental study by Irandoukht et al. (2000). Similar to the trend reported in the experimental investigations (Sagata et al., 2013; Schumann, 2015), this study shows that high calcination temperatures cause a sharp drop in Cu(SA). Based on Fig. 7-a, long or medium aging times should be chosen to obtain high Cu(SA)s. The same recommendation was given in the relevant experimental studies (Farahani et al., 2014; Kniep et al., 2005; Mota et al., 2018; Spencer, 2000; Waller et al., 1989). The results reveal that the 'increasing' pH mode is the worst scenario, leading to the lowest Cu(SA), which is in agreement with the experimental studies available in the literature (Irandoukht et al., 2000; Pan et al., 1988). The experimental results of Pan et al. (1988) imply that 'constant' pH mode is better than 'decreasing' pH mode, leading to higher Cu (SA)s for the catalyst, while Fig. 7 does not convey the same message. Instead, 'decreasing' pH mode results in a higher Cu (SA) than 'constant' pH mode according to Fig. 7-c, showing a higher percentage of purple points (representing 'decreasing' mode) than blue points (representing 'constant' mode) with a positive SHAP value. It follows that 'decreasing' pH mode is better than 'constant' pH mode, which agrees with the experimental results reported by Irandoukht et al. (2000). The SHAP analysis shows that sodium bicarbonate leads to higher Cu(SA)s compared to sodium carbonate, while Irandoukht et al. (2000) reported a different finding based on their experimental study.

Manufacturers of CZA catalyst place a high priority on achieving high Cu(SA)s for this catalyst. Cu(SA) is a useful quantitative measure for a machine learning study, since it has a direct relationship with catalytic activity, and is an inherent characteristic of catalysts, independent of measurement factors. According to the results obtained from the RF classifier, it is possible to estimate the Cu(SA) range with a good accuracy and reliability using smart methods when the synthesis factors are considered as the input features. In addition, the results of

the SHAP analysis reveal the how the synthesis factors affect Cu (SA), thereby providing the manufacturers of CZA catalysts with a better understanding of the synthesis route.

## 6. Conclusions

In this study, Cu(SA) of CZA catalyst is considered as the target variable for classification models based on the synthesis factors. A dataset containing CZA catalyst samples gathered from some publications and patents is used for training three models of RF, SVM, and MLP classifiers. Based on the 10-fold grid search cross-validation approach, the RF classifier outperforms the SVM and MLP classifiers in both training and testing phases. The SHAP analysis reveals the key effects of synthesis factors on Cu(SA) variation as well as on the model response. In a nutshell, the SHAP analysis shows that the optimal conditions to achieve a high Cu(SA) for this catalyst are: sodium bicarbonate should be chosen as the precipitant; pH mode 'decreasing' or 'constant' should be selected (probably 'decreasing' mode is preferable to 'constant' mode); low Cu/Zn ratio; medium or high aging time and temperature; long calcination time; and low or medium calcination temperature. Based on the SHAP analysis, the most influential synthesis factors affecting Cu(SA) value are the Cu/Zn ratio, aging temperature, and Al%.

The relationship between Cu(SA) and the total surface area of the catalyst, which is determined by the BET method (BET(SA)) in the industry, can be interesting to be studied in future work. This proposed study can be conducted using machine learning tools, since measuring the BET(SA) is less expensive and faster than measuring Cu(SA), and finding the relationship mentioned above can lead to an accurate estimation of Cu(SA) and catalytic activity with low cost.

In the present study, the catalyst production method is the co-precipitation. Another industrial production route for this catalyst is precipitation-deposition. Thus, studying the effects of various process and system parameters involved in this method on Cu(SA) can generate useful data/information for CZA catalyst manufacturers.

## Declaration of Competing Interest

The authors declare that they have no known competing financial interests or personal relationships that could have appeared to influence the work reported in this paper.

## References


Álvarez Galván, C., Schumann, J., Behrens, M., Fierro, J.L.G., Schlögl, R., Frei, E., 2016. Reverse water-gas shift reaction at the Cu/ZnO interface: Influence of the Cu/Zn ratio on structure-activity correlations. Appl. Catal. B Environ. 195, 104–111. https://doi.org/10.1016/j.apcatb.2016.05.007

Andache, M., Nemati Kharat, A., Rezaei, M., 2019. Preparation of mesoporous nanocrystalline CuO–ZnO–$Al_2O_3$ catalysts for the $H_2$ purification using catalytic preferential oxidation of CO (CO-PROX). Int. J. Hydrog. Energy 44, 27401–27411. https://doi.org/10.1016/j.ijhydene.2019.08.197

Angelo, L., Kobl, K., Tejada, L.M.M., Zimmermann, Y., Parkhomenko, K., Roger, A.C., 2015. Study of CuZnMOx oxides (M=Al, Zr,Ce,CeZr) for the catalytic hydrogenation of $CO_2$ into methanol. Comptes Rendus Chim. 18, 250–260. https://doi.org/10.1016/j.crci.2015.01.001

Arabloo, M., Bahadori, A., Ghiasi, M.M., Lee, M., Abbas, A., Zendehboudi, S., 2015. A novel modeling approach to optimize oxygen-steam ratios in coal gasification process. Fuel 153, 1–5. https://doi.org/10.1016/j.fuel.2015.02.083

Behrens, M., 2009. Meso- and nano-structuring of industrial Cu/ZnO/($Al_2O_3$) catalysts. J. Catal. 267, 24–29. https://doi.org/10.1016/j.jcat.2009.07.009

Behrens, M., Kasatkin, I., Kühl, S., Weinberg, G., 2010. Phase-pure Cu,Zn,Al hydrotalcite-like materials as precursors for copper rich Cu/ZnO/$Al_2O_3$ catalysts. Chem. Mater. 22, 386–397. https://doi.org/10.1021/cm9029165

Behrens, M., Kniep, B., Kurr, P., Schlogl, R., Hieke, M., 2013a, Methanol synthesis catalyst on the basis of copper, zinc and aluminum. WO 2013/072197 A1.

Behrens, M., Studt, F., Kasatkin, I., Kuhl, S., Havecker, M., Abild-Pedersen, F., Zander, S., Girgsdies, F., Kurr, P., Kniep, B.-L., Tovar, M., Fischer, R.W., Norskov, J.K., Schlogl, R., 2012. The active site of methanol synthesis over Cu/ZnO/$Al_2O_3$ industrial catalysts. Sci. (80-. ) 336, 893–897. https://doi.org/10.1126/science.1219831

Behrens, M., Zander, S., Kurr, P., Jacobsen, N., Senker, J., Koch, G., Ressler, T., Fischer, R.W., Schloegl, R., 2013b. Performance Improvement of Nano-Catalysts by Promoter-Induced Defects in the Support Material: Methanol Synthesis over Cu/ZnO:Al. J. Am. Chem. Soc 135. pp. 6061–6068. https://doi.org/10.1021/ja310456f

Bems, B., Schur, M., Dassenoy, A., Junkes, H., Herein, D., Schlögl, R., 2003. Relations between synthesis and microstructural properties of copper/zinc hydroxycarbonates. Chem. - A Eur. J. 9, 2039–2052. https://doi.org/10.1002/chem.200204122

Breen, J.P., Ross, J.R.H., 1999. Methanol reforming for fuel-cell applications: Development of zirconia-containing Cu-Zn-Al catalysts. Catal. Today 51, 521–533. https://doi.org/10.1016/S0920-5861(99)00038-3

Budiman, A., Ridwan, M., Kim, S.M., Choi, J.W., Yoon, C.W., Ha, J.M., Suh, D.J., Suh, Y.W., 2013. Design and preparation of high-surface-area Cu/ZnO/$Al_2O_3$ catalysts using a modified co-precipitation method for the water-gas shift reaction. Appl. Catal. A Gen. 462, 220–226. https://doi.org/10.1016/j.apcata.2013.05.010

Cai, Y., Davies, S., Wagner, J., 2003, Water gas shift catalyst. US 6,627, 572 Bl. ⟨https://doi.org/10.1074/JBC.274.42.30033⟩.(51).

Cai, Y., Davies, S.L., Jon P., W., 2004, Water gas shift catalyst. US 6,693, 057 B1.

Cavalcanti, F.M., Schmal, M., Giudici, R., Brito Alves, R.M., 2019. A catalyst selection method for hydrogen production through Water-Gas Shift Reaction using artificial neural networks. J. Environ. Manag. 237, 585–594. https://doi.org/10.1016/j.jenvman.2019.02.092

Chamkalani, A., Zendehboudi, S., Chamkalani, R., Lohi, A., Elkamel, A., Chatzis, I., 2013. Utilization of support vector machine to calculate gas compressibility factor. Fluid Phase Equilib. 358, 189–202. https://doi.org/10.1016/j.fluid.2013.08.018

Chawla, N.V., Bowyer, K.W., Hall, L.O., Kegelmeyer, W.P., 2002. SMOTE: synthetic minority over-sampling technique. J. Artif. Intell. Res. 16, 321–357. https://doi.org/10.1613/jair.953

Chinchen, G.C., Hay, C.M., Vandervell, H.D., Waugh, K.C., 1987. The measurement of copper surface areas by reactive frontal chromatography. J. Catal. 103, 79–86. https://doi.org/10.1016/0021-9517(87)90094-7

Christoph, M., 2020, Interpretable Machine Learning A Guide for Making Black Box Models Explainable.

Cross-validation: evaluating estimator performance — scikit-learn [WWW Document], n.d. URL ⟨https://scikit-learn.org/stable/modules/cross_validation.html⟩ (accessed 12.1.22).

Dashti, A., Raji, M., Razmi, A., Rezaei, N., Zendehboudi, S., Asghari, M., 2019. Efficient hybrid modeling of $CO_2$ absorption in aqueous solution of piperazine: Applications to energy and environment. Chem. Eng. Res. Des. 144, 405–417. https://doi.org/10.1016/j.cherd.2019.01.019

Dasireddy, V.D.B.C., Likozar, B., 2019. The role of copper oxidation state in Cu/ZnO/$Al_2O_3$ catalysts in $CO_2$ hydrogenation and methanol productivity. Renew. Energy 140, 452–460. https://doi.org/10.1016/j.renene.2019.03.073

Eduardo, P.F., Damian, C., Fernando, M., 2022. A comparison of deep learning models applied to Water Gas Shift catalysts for hydrogen purification. Int. J. Hydrog. Energy. https://doi.org/10.1016/j.ijhydene.2022.09.215

Farahani, B.V., Rajabi, F.H., Bahmani, M., Ghelichkhani, M., Sahebdelfar, S., 2014. Influence of precipitation conditions on precursor particle size distribution and activity of Cu/ZnO methanol synthesis catalyst. Appl. Catal. A, Gen. https://doi.org/10.1016/j.apcata.2014.05.034

Fierro, J.L.G., Melián-Cabrera, I., López Granados, M., 2002a. Pd-modified Cu-Zn catalysts for methanol synthesis from $CO_2/H_2$

mixtures: Catalytic structures and performance. J. Catal. 210, 285–294. https://doi.org/10.1006/jcat.2002.3677
Fierro, J.L.G., Melián-Cabrera, I., López Granados, M., 2002b. Reverse topotactic transformation of a Cu-Zn-Al catalyst during wet Pd impregnation: Relevance for the performance in methanol synthesis from $CO_2/H_2$ mixtures. J. Catal. 210, 273–284. https://doi.org/10.1006/jcat.2002.3676
Figueiredo, R.T., Santos, M.S., Andrade, H.M.C., Fierro, J.L.G., 2011. Effect of alkali cations on the $CuZnOAl_2O_3$ low temperature water gas-shift catalyst. Catal. Today 172, 166–170. https://doi.org/10.1016/j.cattod.2011.03.073
Fujita, S.I., Moribe, S., Kanamori, Y., Kakudate, M., Takezawa, N., 2001. Preparation of a coprecipitated Cu/ZnO catalyst for the methanol synthesis from $CO_2$ - effects of the calcination and reduction conditions on the catalytic performance. Appl. Catal. A Gen. 207, 121–128. https://doi.org/10.1016/S0926-860X(00)00616-5
Fujitani, T., Nakamura, J., 1998. The effect of ZnO in methanol synthesis catalysts on Cu dispersion and the specific activity. Catal. Lett. 56, 119–124. https://doi.org/10.1023/a:1019000927366
Gherardi, P., Ruggeri, O., Trifiro, F., Vaccari, A., Del Piero, G., Manara, G., Notari, A., 1983, Preparation of Cu-Zn-Al Mixed Hydroxycarbonates Precursors of Catalysts for the Synthesis of Methanol at Low Pressure 723–733. ⟨https://doi.org/10.1016/S0167–2991(09)60062–8⟩.
Ghiasi, M.M., Bahadori, A., Zendehboudi, S., Chatzis, I., 2015. Rigorous models to optimise stripping gas rate in natural gas dehydration units. Fuel 140, 421–428. https://doi.org/10.1016/j.fuel.2014.09.084
Ghiasi, M.M., Zendehboudi, S., 2021. Application of decision tree-based ensemble learning in the classification of breast cancer. Comput. Biol. Med. 128, 104089. https://doi.org/10.1016/j.compbiomed.2020.104089
Giussani, A., 2019, Applied Machine Learning with Python, Logo s.r.l., Borgoricco (Padua).
Golbabaei, M.H., Saeidi Varnoosfaderani, M., Zare, A., Salari, H., Hemmati, F., Abdoli, H., Hamawandi, B., 2022. Performance Analysis of Anode-Supported Solid Oxide Fuel Cells: A Machine Learning Approach. Mater. (Basel) 15, 7760. https://doi.org/10.3390/ma15217760
Guil-López, R., Mota, N., Llorente, J., Millán, E., Pawelec, B., García, R., Fierro, J.L.G., Navarro, R.M., 2020. Structure and activity of Cu/ZnO catalysts co-modified with aluminium and gallium for methanol synthesis. Catal. Today 355, 870–881. https://doi.org/10.1016/j.cattod.2019.03.034
Günay, M.E., Akpinar, F., Onsan, Z.I., Yildirim, R., 2012. Investigation of water gas-shift activity of Pt-MOx-$CeO_2/Al_2O_3$ (M = K, Ni, Co) using modular artificial neural networks. Int. J. Hydrog. Energy 37, 2094–2102. https://doi.org/10.1016/j.ijhydene.2011.09.148
Gunay, M.E., Yildirim, R., 2011. Neural network Analysis of Selective CO Oxidation over Copper-Based Catalysts for Knowledge Extraction from Published Data in the Literature. Am. Chem. Soc. 12488–12500. https://doi.org/10.1021/ie2013955
Günay, M.E., Yildirim, R., 2013. Developing global reaction rate model for CO oxidation over Au catalysts from past data in literature using artificial neural networks. Appl. Catal. A Gen. 468, 395–402. https://doi.org/10.1016/j.apcata.2013.08.056
Günter, M.M., Ressler, T., Bems, B., Büscher, C., Genger, T., Hinrichsen, O., Muhler, M., Schlögl, R., 2001. Implication of the microstructure of binary Cu/ZnO catalysts for their catalytic activity in methanol synthesis. Catal. Lett. 71, 37–44. https://doi.org/10.1023/A:1016696022840
Guo, P., Chen, L., Yang, Q., Qiao, M., Li, H., Li, H., Xu, H., Fan, K., 2009. Cu/ZnO/Al2O3 water–gas shift catalysts for practical fuel cell applications: the performance in shut-down/start-up operation. Int. J. Hydrogen Energy 34. pp. 2361–2368.⟨https://doi.org/10.1016/J.IJHYDENE.2008.12.081⟩.
Gusi, S., Trifirò, F., Vaccari, A., Del Piero, G., 1985. Catalysts for low-temperature methanol synthesis. II. Catalytic behavior of Cu/Zn/Al mixed oxides. J. Catal. 94, 120–127. https://doi.org/10.1016/0021-9517(85)90087-9
Irandoukht, A., Sohrabi, M., Mandegarian, R., 2000. Effect of Preparation Parameters on the Activity of Methanol Synthesis Catalysts: A Laboratory Scale Study. React. Kinet. Catal. Lett. 70, 259–264. https://doi.org/10.1023/A:1010328613993
Jeong, C., Ham, H., Bae, J.W., Kang, D.C., Shin, C.H., Baik, J.H., Suh, Y.W., 2017. Facile structure tuning of a methanol-synthesis catalyst towards the direct synthesis of dimethyl ether from syngas. Chem. Cat. Chem. 9, 4484–4489. https://doi.org/10.1002/cctc.201701167
Jeong, D.W., Jang, W.J., Shim, J.O., Han, W.B., Roh, H.S., Jung, U.H., Yoon, W.L., 2014. Low-temperature water-gas shift reaction over supported Cu catalysts. Renew. Energy 65, 102–107. https://doi.org/10.1016/j.renene.2013.07.035
Kamari, A., Bahadori, A., Mohammadi, A.H., Zendehboudi, S., 2015. New tools predict monoethylene glycol injection rate for natural gas hydrate inhibition. J. Loss Prev. Process Ind. 33, 222–231. https://doi.org/10.1016/j.jlp.2014.12.013
Kamari, A., Mohammadi, A.H., Bahadori, A., Zendehboudi, S., 2014. Prediction of air specific heat ratios at elevated pressures using a novel modeling approach. Chem. Eng. Technol. 37, 2047–2055. https://doi.org/10.1002/ceat.201400261
Khzouz, M., Wood, J., Pollet, B., Bujalski, W., 2013. Characterization and activity test of commercial $Ni/Al_2O_3$, $Cu/ZnO/Al_2O_3$ and prepared $Ni–Cu/Al_2O_3$ catalysts for hydrogen production from methane and methanol fuels. Int. J. Hydrog. Energy 38, 1664–1675. https://doi.org/10.1016/J.IJHYDENE.2012.07.026
Kim, J., Jeong, C., Baik, J.H., Suh, Y.W., 2020. Phases of Cu/Zn/Al/Zr precursors linked to the property and activity of their final catalysts in $CO_2$ hydrogenation to methanol. Catal. Today 347, 70–78. https://doi.org/10.1016/j.cattod.2018.09.008
Kim, S.M., Lee, M.E., Choi, J.W., Suh, D.J., Suh, Y.W., 2011. Role of ZnO in $Cu/ZnO/Al_2O_3$ catalyst for hydrogenolysis of butyl butyrate. Catal. Commun. 12, 1328–1332. https://doi.org/10.1016/j.catcom.2011.05.006
Kniep, B.L., Girgsdies, F., Ressler, T., 2005. Effect of precipitate aging on the microstructural characteristics of Cu/ZnO catalysts for methanol steam reforming. J. Catal. 236, 34–44. https://doi.org/10.1016/j.jcat.2005.09.001
Kurr, P., Kasatkin, I., Girgsdies, F., Trunschke, A., Schlögl, R., Ressler, T., 2008. Microstructural characterization of $Cu/ZnO/Al_2O_3$ catalysts for methanol steam reforming-A comparative study. Appl. Catal. A Gen. 348, 153–164. https://doi.org/10.1016/j.apcata.2008.06.020
Kurtz, M., Bauer, N., Büscher, C., Wilmer, H., Hinrichsen, O., Becker, R., Rabe, S., Merz, K., Driess, M., Fischer, R.A., Muhler, M., 2004. New synthetic routes to more active Cu/ZnO catalysts used for methanol synthesis. Catal. Lett. 92, 49–52. https://doi.org/10.1023/B:CATL.0000011085.88267.a6
Kurtz, M., Wilmer, H., Genger, T., Hinrichsen, O., Muhler, M., 2003. Deactivation of supported copper catalysts for methanol synthesis. Catal. Lett. 86, 77–80. https://doi.org/10.1023/A:1022663125977
Lindstrom, B., Pettersson, L.J., 2001, Hydrogen generation by steam reforming of methanol over copper-based catalysts for fuel cell applications 26, 923–933. ⟨https://doi.org/10.1016/S0360–3199(01)00034–9⟩.
Lundberg, S.M., Erion, G., Chen, H., DeGrave, A., Prutkin, J.M., Nair, B., Katz, R., Himmelfarb, J., Bansal, N., Lee, S.-I., 2020. From local explanations to global understanding with explainable AI for trees. Nat. Mach. Intell. 2, 56–67. https://doi.org/10.1038/s42256-019-0138-9
Lundberg, S.M., Lee, S.-I., 2017, A Unified Approach to Interpreting Model Predictions, in: 31st Conference on Neural Information Processing Systems (NIPS 2017). pp. 1208–1217.
Madon, R.J., Nagel, P., 2009, Low temperature water gas shift catalyst. US 2009/0149324 A1.
Meshkini, F., Taghizadeh, M., Bahmani, M., 2010. Investigating the effect of metal oxide additives on the properties of $Cu/ZnO/Al_2O_3$ catalysts in methanol synthesis from syngas using factorial experimental design. Fuel 89, 170–175. https://doi.org/10.1016/j.fuel.2009.07.007
Miah, M.I., Zendehboudi, S., Ahmed, S., 2020. Log data-driven model and feature ranking for water saturation prediction using machine learning approach. J. Pet. Sci. Eng. 194, 107291. https://doi.org/10.1016/j.petrol.2020.107291
Mota, N., Guil-Lopez, R., Pawelec, B.G., Fierro, J.L.G., Navarro, R.M., 2018. Highly active Cu/ZnO-Al catalyst for methanol synthesis: Effect of aging on its structure and activity. RSC Adv. 8, 20619–20629. https://doi.org/10.1039/c8ra03291b
Odabaşi, Ç., Günay, M.E., Yildirim, R., 2014. Knowledge extraction for water gas shift reaction over noble metal catalysts from publications in the literature between 2002 and 2012. Int. J. Hydrog. Energy 39, 5733–5746. https://doi.org/10.1016/j.ijhydene.2014.01.160
Omata, K., Umegaki, T., Ishiguro, G., Yamada, M., 2001. Optimization of Cu-Zn-Al oxide catalyst for methanol synthesis using genetic algorithm. J. Jpn. Pet. Inst. 44, 327–331. https://doi.org/10.1627/jpi1958.44.327

Pan, W.X., Cao, R., Roberts, D.L., Griffin, G.L., 1988. Methanol synthesis activity of Cu/ZnO catalysts. J. Catal. 114, 440–446. https://doi.org/10.1016/0021-9517(88)90047-4

Park, J., Kim, J., Baik, J.H., Suh, Y., Jeong, C., 2018. Effects of Al3+ precipitation onto primitive amorphous Cu-Zn precipitate on methanol synthesis over Cu/ZnO/$Al_2O_3$ catalyst. Korean J. Chem. Eng. 35, 3–8. https://doi.org/10.1007/s11814-018-0186-6

Porta, P., Rossi, S., De, Giovanni, F., Jacono, M., Lo, Minelli, G., Moretti, G., 1988. Structural Characterization of Malachite-like Coprecipitated Precursors of Binary CuO-ZnO Catalysts. J. Catal. 109, 367–377. https://doi.org/10.1016/0021-9517(88)90219-9

Pospelova, V., Aubrecht, J., Kikhtyanin, O., Pacultová, K., Kubička, D., 2019. CuZn catalysts superior to adkins catalysts for dimethyl adipate hydrogenolysis. ChemCatChem 11, 2169–2178. https://doi.org/10.1002/cctc.201900334

Pospelova, V., Aubrecht, J., Pacultová, K., Lhotka, M., Kikhtyanin, O., Kubička, D., 2020. Does the structure of CuZn hydroxycarbonate precursors affect the intrinsic hydrogenolysis activity of CuZn catalysts? Catal. Sci. Technol. 10, 3303–3314. https://doi.org/10.1039/d0cy00143k

Reubroycharoen, P., Vitidsant, T., Yoneyama, Y., Tsubaki, N., 2004. Development of a new low-temperature methanol synthesis process. Catal. Today 89, 447–454. https://doi.org/10.1016/j.cattod.2004.01.006

Safari, H., Shokrollahi, A., Jamialahmadi, M., Ghazanfari, M.H., Bahadori, A., Zendehboudi, S., 2014. Prediction of the aqueous solubility of $BaSO_4$ using pitzer ion interaction model and LSSVM algorithm. Fluid Phase Equilib. 374, 48–62. https://doi.org/10.1016/j.fluid.2014.04.010

Sagata, K., Imazu, N., Yahiro, H., 2013. Study on factors controlling catalytic activity for low-temperature water-gas-shift reaction on Cu-based catalysts. Catal. Today 201, 145–150. https://doi.org/10.1016/j.cattod.2012.03.064

Saito, M., Fujitani, T., Takeuchi, M., Watanabe, T., 1996. Development of copper/zinc oxide-based multicomponent catalysts for methanol synthesis from carbon dioxide and hydrogen. Appl. Catal. A Gen. 138, 311–318. https://doi.org/10.1016/0926-860X(95)00305-3

Samei, E., Taghizadeh, M., Bahmani, M., 2012. Enhancement of stability and activity of Cu/ZnO/$Al_2O_3$ catalysts by colloidal silica and metal oxides additives for methanol synthesis from a $CO_2$-rich feed. Fuel Process. Technol. 96, 128–133. https://doi.org/10.1016/j.fuproc.2011.12.028

Schumann, J., Lunkenbein, T., Tarasov, A., Thomas, N., Schlögl, R., Behrens, M., 2014. Synthesis and Characterisation of a Highly Active Cu/ZnO:Al Catalyst. ChemCatChem 6, 2889–2897. https://doi.org/10.1002/cctc.201402278

Schumann, J., 2015. Cu, Zn-based catalysts for methanol synthesis. Tech. Univ. Berl., PhD Thesis, 156 pages. https://doi.org/10.14279/depositonce-4391

Shen, G.C., Fujita, S.I., Matsumoto, S., Takezawa, N., 1997. Steam reforming of methanol on binary CU/ZnO catalysts: Effects of preparation condition upon precursors, surface structure and catalytic activity. J. Mol. Catal. A Chem. 124, 123–136. https://doi.org/10.1016/S1381-1169(97)00078-2

Shim, J.O., Na, H.S., Ahn, S.Y., Jeon, K.W., Jang, W.J., Jeon, B.H., Roh, H.S., 2019. An important parameter for synthesis of $Al_2O_3$ supported Cu-Zn catalysts in low-temperature water-gas shift reaction under practical reaction condition. Int. J. Hydrog. Energy 44, 14853–14860. https://doi.org/10.1016/j.ijhydene.2019.04.042

Shishido, T., Yamamoto, M., Li, D., Tian, Y., Morioka, H., Honda, M., Sano, T., Takehira, K., 2006. Water-gas shift reaction over Cu/ZnO and Cu/ZnO/Al2O3 catalysts prepared by homogeneous precipitation. Appl. Catal. A Gen. 303, 62–71. https://doi.org/10.1016/j.apcata.2006.01.031

Shokrani, R., Haghighi, M., Jodeiri, N., Ajamein, H., Abdollahifar, M., 2014. Fuel cell grade hydrogen production via methanol steam reforming over CuO/ZnO/$Al_2O_3$ nanocatalyst with various oxide ratios synthesized via urea-nitrates combustion method. Int. J. Hydrog. Energy 39, 13141–13155. https://doi.org/10.1016/J.IJHYDENE.2014.06.048

Sklearn.preprocessing.StandardScaler — scikit-learn 1.1.3 documentation [WWW Document], n.d. URL ⟨https://scikit-learn.org/stable/modules/generated/sklearn.preprocessing.StandardScaler.html#sklearn.preprocessing.StandardScaler⟩ (accessed 12.6.22).

Sklearn.utils.resample — scikit-learn 1.1.3 documentation [WWW Document], n.d. URL ⟨https://scikit-learn.org/stable/modules/generated/sklearn.utils.resample.html⟩ (accessed 12.5.22).

Smith, A., Keane, A., Dumesic, J.A., Huber, G.W., Zavala, V.M., 2020. A machine learning framework for the analysis and prediction of catalytic activity from experimental data. Appl. Catal. B Environ. 263, 118257. https://doi.org/10.1016/j.apcatb.2019.118257

Smith, P.J., Kondrat, S.A., Chater, P.A., Yeo, B.R., Shaw, G.M., Lu, L., Bartley, J.K., Taylor, S.H., Spencer, M.S., Kiely, C.J., Kelly, G.J., Park, C.W., Hutchings, G.J., 2017. A new class of Cu/ZnO catalysts derived from zincian georgeite precursors prepared by co-precipitation. Chem. Sci. 8, 2436–2447. https://doi.org/10.1039/c6sc04130b

Spencer, M.S., 2000. Precursors of copper/zinc oxide catalysts. Catal. Lett. 66, 255–257. https://doi.org/10.1023/A:1019076329319

Stone, Frank S., Waller, D., 2003a. Cu–ZnO and Cu–ZnO/$Al_2O_3$ catalysts for the reverse water-gas shift reaction. The effect of the Cu/Zn ratio on precursor characteristics and on the activity of the derived catalysts. Top. Catal. 22. https://doi.org/10.1023/A:1023592407825

Stone, Frank S., Waller, D., 2003b. Cu-ZnO and Cu-ZnO/$Al_2O_3$ catalysts for the reverse water-gas shift reaction. The effect of the Cu/Zn ratio on precursor characteristics and on the activity of the derived catalysts. Top. Catal. 22, 305–318. https://doi.org/10.1023/A:1023592407825

Studt, F., Behrens, M., Abild-Pedersen, F., 2014. Energetics of the water-gas-shift reaction on the active sites of the industrially used Cu/ZnO/$Al_2O_3$ catalyst. Catal. Lett. 144, 1973–1977. https://doi.org/10.1007/s10562-014-1363-9

Talebi, R., Ghiasi, M.M., Talebi, H., Mohammadyian, M., Zendehboudi, S., Arabloo, M., Bahadori, A., 2014. Application of soft computing approaches for modeling saturation pressure of reservoir oils. J. Nat. Gas. Sci. Eng. 20, 8–15. https://doi.org/10.1016/j.jngse.2014.04.023

Umegaki, T., Masuda, A., Omata, K., Yamada, M., 2008. Development of a high performance Cu-based ternary oxide catalyst for oxidative steam reforming of methanol using an artificial neural network. Appl. Catal. A Gen. 351, 210–216. https://doi.org/10.1016/j.apcata.2008.09.019

Waller, D., Stirling, D., Stone, F.S., Spencer, M.S., 1989. Copper-zinc oxide catalysts: Activity in relation to precursor structure and morphology. Faraday Discuss. Chem. Soc. 87, 107–120. https://doi.org/10.1039/DC9898700107

Wang, G., Zuo, Y., Han, M., Wang, J., 2010. Copper crystallite size and methanol synthesis catalytic property of Cu-based catalysts promoted by Al, Zr and Mn. React. Kinet. Mech. Catal. 101, 443–454. https://doi.org/10.1007/s11144-010-0240-9

Wilmer, H., Genger, T., Hinrichsen, O., 2003. The interaction of hydrogen with alumina-supported copper catalysts: a temperature-programmed adsorption / temperature-programmed desorption / isotopic exchange reaction study. J. Catal. 215, 188–198. https://doi.org/10.1016/S0021-9517(03)00003-4

Xu, L., Peng, D., Liu, W., Feng, Y., Hou, Y., Li, X., Huang, C., 2018, A Modified Co-precipitation Method to Prepare Cu/ZnO/Al2O3 Catalyst and Its Application in Low Temperature Water-gas Shift (LT-WGS) Reaction. J. Wuhan Univ. Technol. Mater. Sci. Ed. 33, 876–883. ⟨https://doi.org/10.1007/s11595–018-1907–8⟩.

Zander, S., Kunkes, E.L., Schuster, M.E., Schumann, J., Weinberg, G., Teschner, D., Jacobsen, N., Schlçgl, R., Behrens, M., 2013. The Role of the Oxide Component in the Development of Copper Composite Catalysts for Methanol Synthesis. Angew. Chem. 52, 6536–6540. https://doi.org/10.1002/anie.201301419

Zendehboudi, S., Rezaei, N., Lohi, A., 2018. Applications of hybrid models in chemical, petroleum, and energy systems: A systematic review. Appl. Energy 228, 2539–2566. https://doi.org/10.1016/j.apenergy.2018.06.051

Zhang, C., Yang, H., Gao, P., Zhu, H., Zhong, L., Wang, H., Wei, W., Sun, Y., 2017. Preparation and $CO_2$ hydrogenation catalytic properties of alumina microsphere supported Cu-based catalyst by deposition-precipitation method. J. $CO_2$ Util. 17, 263–272. https://doi.org/10.1016/j.jcou.2016.11.015

Zhang, L., Li, F., Evans, D., Duan, X., 2010. Cu–Zn–(Mn)–(Fe)–Al layered double hydroxides and their mixed metal oxides: physicochemical and catalytic properties in wet hydrogen peroxide oxidation of phenol. Ind. Eng. Chem. Res. 49, 5959–5968. https://doi.org/10.1021/ie9019193

Zhu, J., Araya, S.S., Cui, X., Kær, S.K., 2022. The role of effectiveness factor on the modeling of methanol steam reforming over CuO/ZnO/$Al_2O_3$ catalyst in a multi-tubular reactor. Int. J. Hydrog. Energy 47, 8700–8715. https://doi.org/10.1016/J.IJHYDENE.2021.12.223